



Low temperature annealing of nanocrystalline Si paste for pn junction formation

Yusuke Kuboki ^a, Huan Zhu ^a, Morihiro Sakamoto ^a, Hiroshige Matsumoto ^b, Kungen Teii ^c, Yoshimine Kato ^{d,*}

^a Department of Automotive Science, Graduate School of Integrated Frontier Science, Kyushu University, Fukuoka, 819-0395, Japan

^b Electrochemical Energy Conversion Division, International Institute for Carbon-Neutral Energy Research, Kyushu University, Fukuoka, 819-0395, Japan

^c Department of Applied Science for Electronics and Materials, Kyushu University, Kasuga, Fukuoka, 816-8580, Japan

^d Faculty of Engineering, Kyushu University, Fukuoka, 819-0395, Japan



ARTICLE INFO

Keywords:

Si paste
pn junction
Aluminum-induced crystallization (AIC)
Oxidation
Crystallization
Annealing

ABSTRACT

Low temperature annealing of p- and n-type Si paste films consisting of nanocrystal Si particles coated on Al substrates was investigated for application to low cost large-area electronic devices such as solar cells. This process based on aluminum-induced-crystallization enabled one to enhance recrystallization of the Si paste films with reduction of residual tensile stress while suppressing oxidation greatly even at low temperatures (400–550 °C), as confirmed by Raman spectroscopy, X-ray diffraction, and Fourier-transform infrared spectroscopy. pn homo-junction diodes were fabricated successfully using a p/n-type double layer Si paste film and even an n-type single layer Si paste film on Al substrates by annealing at temperatures less than 550 °C. The current-voltage characteristic of the diode using a p/n-type double layer Si paste film showed rectification with the on/off current ratio of about 3200 and the reverse current density of the order of 10^{-9} A/cm² at room temperature.

1. Introduction

Silicon (Si), as one of leading electronic materials, is widely employed in almost every aspect of electronic industries due to the high material quality and widespread technological know-how [1,2]. Unlike the computer industry, the large-area electronic devices such as liquid crystal displays and solar cells can endure larger feature sizes even by using lower quality Si instead of high-quality crystalline Si (c-Si) wafers [3]. In order to lower the manufacturing cost, several high-throughput manufacturing techniques such as deposition of a-Si films and dropping Si paste made of Si nanocrystals dispersed in solvents that can be adopted [4]. However, the use of a-Si films tends to degrade performance of electronic devices because of a relatively low carrier mobility of ~ 0.5 cm²/V·s [5], thus limiting its application. Besides, chemical vapor deposition as the typical manufacturing technique of a-Si films costs high because of requirement of vacuum equipment [6].

Utilizing Si paste fabricated by Si nanocrystals is an another feasible approach for manufacturing large area electronic devices. The manufacturing cost of Si pastes is generally much lower than c-Si wafers

because the conventional Si ingot growth and sawing process can be skipped. Although there are some reports on doping of Si paste toward application for solar cells [7,8], Si paste has been merely used as a device component by combining with a c-Si wafer for producing back-surface-field (BSF). The heavily B-doped Si paste with a dopant concentration up to the order of 10^{21} cm⁻³ was screen printed on the rear side of a p-type Si wafer, and the laser doping method was adopted to form a p⁺ region [8]. An electric field was also formed at the p⁺/p interface, which introduces a barrier to minority carrier flow at the rear surface, thus increasing the open circuit voltage [9].

In our previous study, an attempt was made to fabricate a whole device using both p- and n-type Si paste films without using a c-Si wafer [10]. The resulting pn homo-junction device showed rectification characteristics only when the doped Si paste was annealed at a temperature of 1100 °C for enhancing crystallization. On the other hand, the Si paste composed of Si nanocrystals was found to be oxidized easily even in high purity Ar gas atmosphere due to the high surface to volume ratio. We recently developed a rapid thermal annealing (RTA) technique to reduce the degree of oxidation of Si paste and improve rectification

* Corresponding author.

E-mail address: kato.yoshimine.434@m.kyushu-u.ac.jp (Y. Kato).

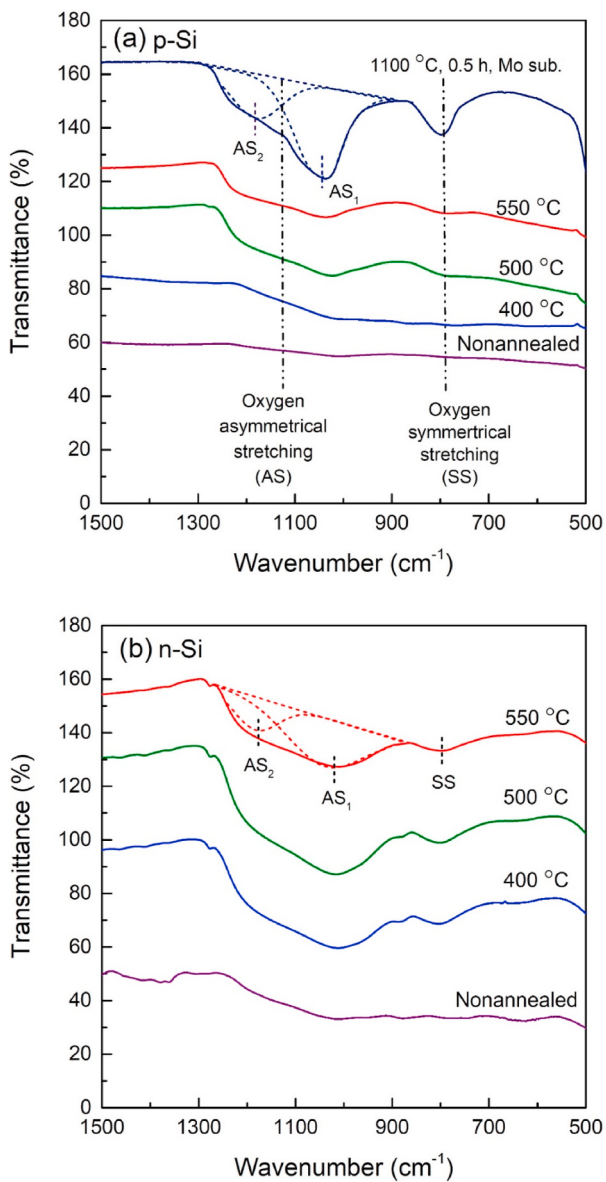


Fig. 1. FT-IR spectra of the (a) p- and (b) n-type Si paste films on Al substrates before and after annealing at 400, 500, and 550 °C. The spectrum for the p-type film on a Mo substrate annealed at 1100 °C for 0.5 h is given in (a) as a reference.

characteristics of the pn homo-junction device [11]. Nevertheless, it is still desired to develop the RTA technique at lower temperatures for suppressing oxidation fundamentally.

Metal-induced crystallization is a promising process to crystallize an amorphous Si (a-Si) film at temperatures below 600 °C by using metal species such as Au, Al, and Ni [12]. Al is considered to be most favorable because it plays a multiple role such as back contact electrode and BSF in solar cells [13]. Nast et al. showed that, after annealing of an a-Si film on an Al layer at 600 °C or less, a c-Si layer appeared under the Al layer [14]. Additionally, Si grains started nucleation primarily at the Al/a-Si interface, where the Al grain boundaries met reduction of the free energy [15]. In this paper, Si paste films consisting of Si nanocrystals are fabricated by using a planetary ball milling from the source materials. The process based on Al-induced crystallization (AIC) is utilized for enhancing recrystallization of Si paste films at low temperatures to suppress oxidation of the Si paste, and improve rectification characteristics of the pn junction devices using the Si paste.

2. Experimental methods

p- and n-type Si pastes were produced from p- and n-type c-Si (100) wafers with room-temperature resistivities of 6.5–7.3 mΩ cm (B doped, carrier density of 10^{19} cm^{-3}) and 13–16 mΩ cm (Sb doped, carrier density of $6 \times 10^{18} \text{ cm}^{-3}$), respectively. First, the c-Si wafer was grinded manually into fine powder in a nitrogen filled glove box in order to prevent oxidation. Second, the Si powder dissolved in acetonitrile solution was transferred to ZrO₂ milling pot with ZrO₂ milling beads of 2 mm in diameter. Afterwards, the milling pot was filled with inert 6N Ar gas. During the milling process, the Si powder was spalled by a planetary ball miller (Fritsch Pulverisette 7 classic line) at a rotation speed of 500 rpm for 1 h.

Al substrates with a size of $10 \times 10 \text{ mm}^2$ were used in the experiment. Prior to dropping of the Si paste, the Al substrate was ultrasonically cleaned in ethanol. Two types of junction device were fabricated using the Si paste. First, 20 µl of p- and n-type Si pastes were sequentially coated on the Al substrate. Second, 20 µl of n-type Si paste was only coated on the Al substrate. All Si paste films were naturally dried in a N₂ filled glove box. In order to reduce the internal porosity of the Si paste films, pressing was applied using an oil hydraulic presser at a load of approximately 13 kN. For subsequent annealing treatment, the Si paste films were placed in a quartz tube of 52 cm in length and 1.4 cm in inner diameter with flowing 6N Ar gas at a rate of 0.7 L/min at atmospheric pressure. The films were then annealed in a conventional tubular furnace at 400, 500, and 550 °C for 3 h. After the annealing, the films were etched with 3 wt % HF solution for 1 min to remove the native oxide. Finally, electrodes were formed on the films using silver paste.

Fourier-transform infrared spectroscopy (FT-IR, PerkinElmer Spectrum Two) was used to examine the degree of oxidation of the Si paste films. Raman spectroscopy (Nano-photon RAMAN touch) and X-ray diffraction (XRD, Rigaku Ultima IV) were used to examine the crystallinity of the Si paste films. Raman spectra were measured with a 532 nm-wavelength excitation laser. XRD patterns were measured with Cu K α radiation ($\lambda = 1.54 \text{ \AA}$). The surface morphology and element distribution of the Si paste films were observed by scanning electron microscopy (SEM, Hitachi SU6600) equipped with an energy dispersive X-ray spectrometer (EDX, Apollo XLT SDD). Current-voltage (I-V) characteristics of the pn junction devices were measured by using a power device analyzer/curve tracer (Agilent Technologies B1505A) at room temperature in a vacuum.

3. Results and discussion

Fig. 1 (a) and (b) show the FT-IR spectra of the p- and n-type Si paste films on Al substrates before and after annealing at temperatures of 400, 500, and 550 °C. The spectrum for the p-type film on a Mo substrate annealed at 1100 °C for 0.5 h is also shown as a reference [10]. There are a lot of research on IR absorption characteristics of SiO₂ and they can be summarized as three major vibration modes: rocking, symmetrical stretching (SS) and asymmetrical stretching (AS) motion of oxygen atoms in the Si–O–Si bonds [16–18]. The dominant peak in a transmittance spectrum of SiO₂ is attributed to the AS motion of oxygen atoms, which has a broad absorption peak at around 1120 cm⁻¹. More specifically, the peak of stretching band located at lower frequency (near 1050 cm⁻¹) is the so-called AS₁ vibrational mode (in phase motion of oxygen atoms), while the 1180 cm⁻¹ peak is the AS₂ vibrational mode (out of phase motion of oxygen atoms) [19]. As the annealing temperature rises, an absorption peak near 800 cm⁻¹ attributed to the SS vibration mode appears. The rocking vibration mode located at around 500 cm⁻¹ is slightly observed in **Fig. 1(a)**.

To compare the degree of oxidation of the Si paste films before and after annealing, the peak areas of the AS and SS modes were calculated. For p-type Si paste films, the peak areas for the films on Al are much smaller than the film on the Mo substrate annealed at higher temperature. This means that the degree of oxidation is reduced greatly by

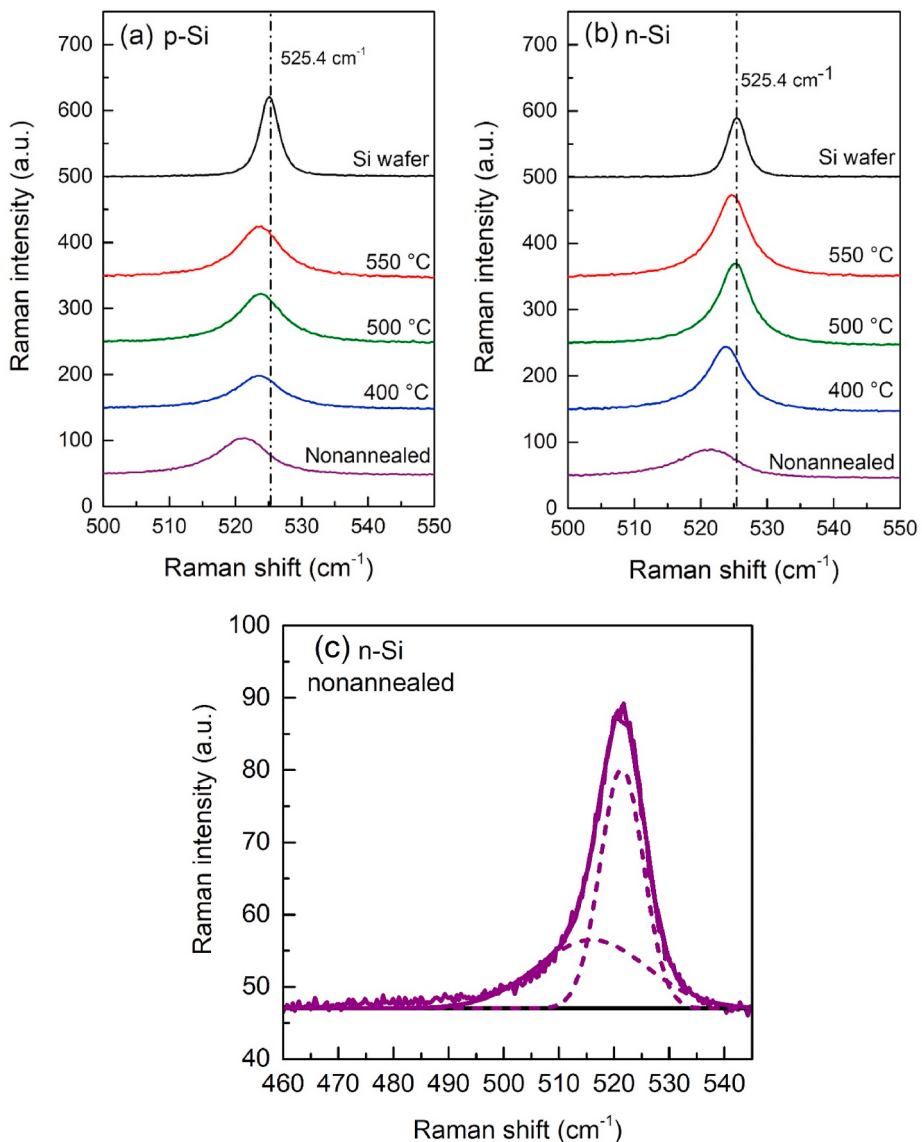


Fig. 2. Raman spectra of the (a) p- and (b) n-type Si paste films on Al substrates before and after annealing at 400, 500, and 550 °C. The spectrum for a c-Si wafer is given in (a) and (b) as a reference. (c) Typical fitting of the 521 cm⁻¹ peak for the film before annealing using two Gaussian distribution functions.

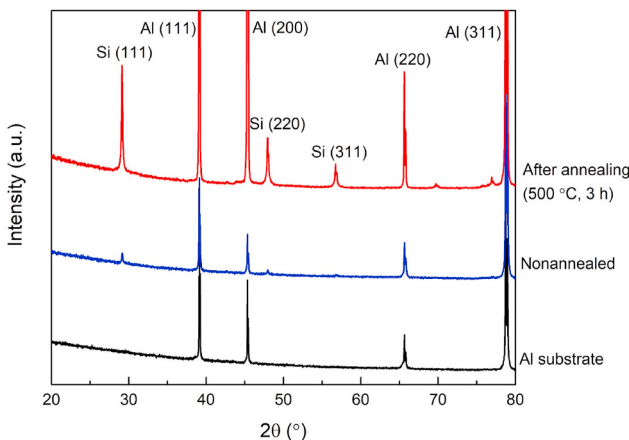


Fig. 3. XRD patterns of the p-type Si paste films on Al substrates before and after annealing at 500 °C. The XRD pattern of an Al substrate is given as a reference.

lowering the annealing temperature from 1100 °C down to 400 °C despite an increase in annealing time from 0.5 to 3 h. In contrast, the peak areas for the n-type Si paste films on Al are large, almost comparable with the film on Mo. It is considered that the oxidation rate of Sb doped Si is higher than B doped Si below 1000 °C even with a lower dopant concentration, through comparison of oxidizability of Sb, P, and B doped Si [20,21]. A higher oxidizability of Sb doped Si is attributed to a lower degree of crystal perfection as follows: (1) acceptor impurities (Al, B, Ga, and In) are depleted near the Si surface, while donor impurities (As, P, and Sb) are piled up near the Si surface [20], thus introducing larger lattice distortion into the surface, and (2) due to the large atomic radius of Sb (0.136 nm) relative to Si (0.117 nm), Sb doping causes heavier lattice strain in the Si bulk, thus introducing excess vacancies into the bulk [21].

It is interesting to note that the peak areas for the film annealed at 550 °C are rather smaller than that at 500 °C, indicating less oxidation. This could be due to grain boundary diffusion of Al from the substrate to the film as also shown later by EDX. A diffusion coefficient tends to increase exponentially with temperature, following an Arrhenius type relation [22–24]. It is reasonable to consider that Al atoms in the film annealed at 550 °C diffuse faster and fill more into the pores. These Al

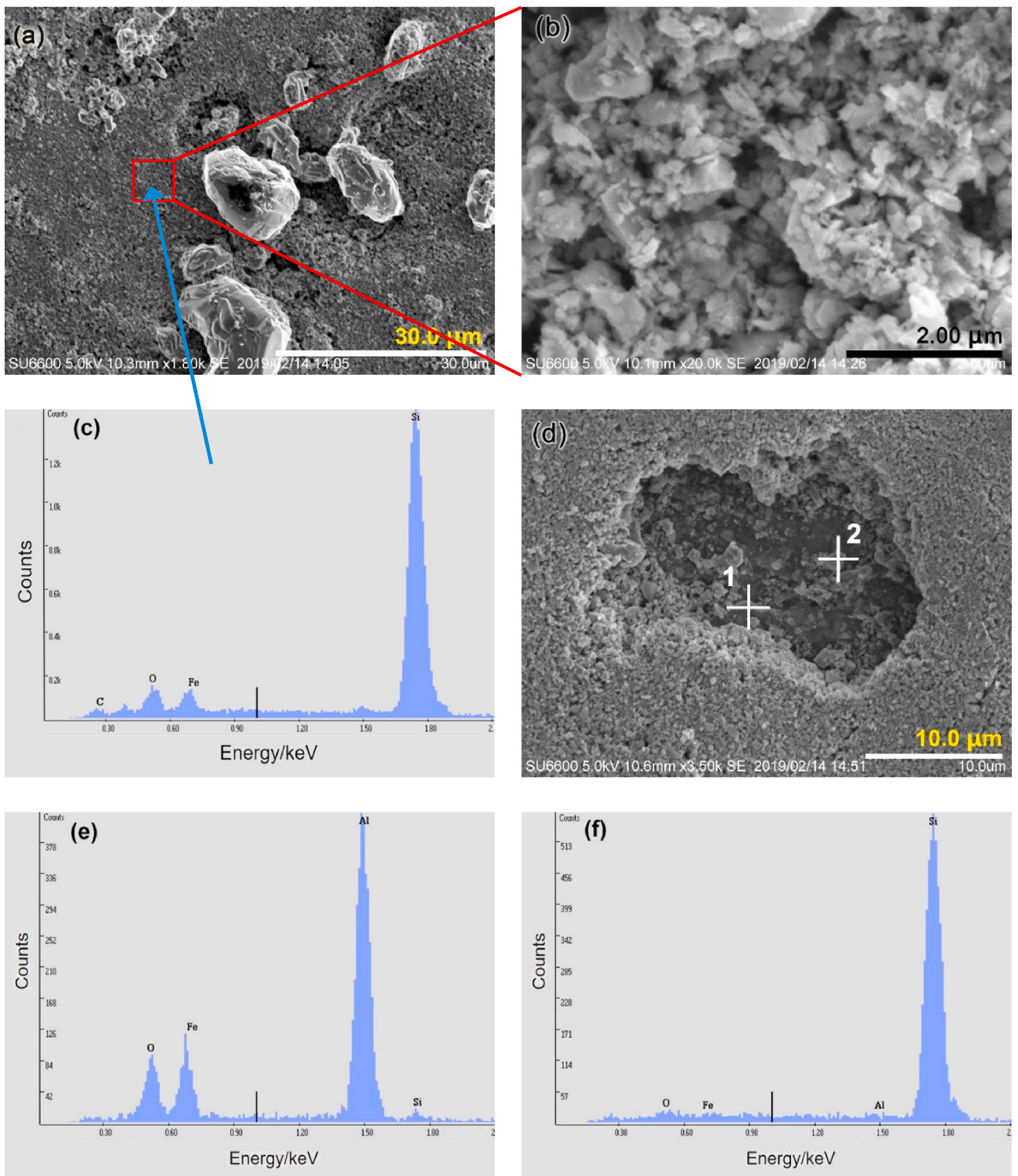


Fig. 4. (a) SEM image of the surface morphology of the p-type Si paste film on an Al substrate annealed at 500 °C. (b) Higher magnification SEM image and (c) EDX spectrum of the square part of (a). SEM image of a hollow-like region [(d)] and EDX spectra for two positions marked with cross symbols 1 [(e)] and 2 [(f)] in (d).

atoms filling into the pores prevent Si atoms from contacting with remaining air in the pores. On the other hand, as the Ellingham diagram [25] indicates that O atoms are more likely to react with Al than Si, Al atoms could be the sacrificial substance of oxidation instead of Si.

The Raman spectra of the p and n-type Si paste films on Al substrates before and after annealing at temperatures of 400, 500, and 550 °C are shown in Fig. 2 (a) and 2 (b), respectively. The spectrum for a c-Si wafer is also shown as a reference. While the peak position of the Si paste film

before annealing is centered at around 521 cm⁻¹, that after annealing shifts to higher wavenumbers towards 525.4 cm⁻¹ for c-Si. This could be due to the relaxation of tensile stress in the Si paste film, which resulted from distortion of Si lattice by ball milling process [26]. The peak shape of the films after annealing becomes sharper as its full width at half maximum (FWHM) actually becomes closer to that of c-Si, confirming an increase in crystallinity by annealing.

The typical fitting of the 521 cm⁻¹ peak for the film before annealing

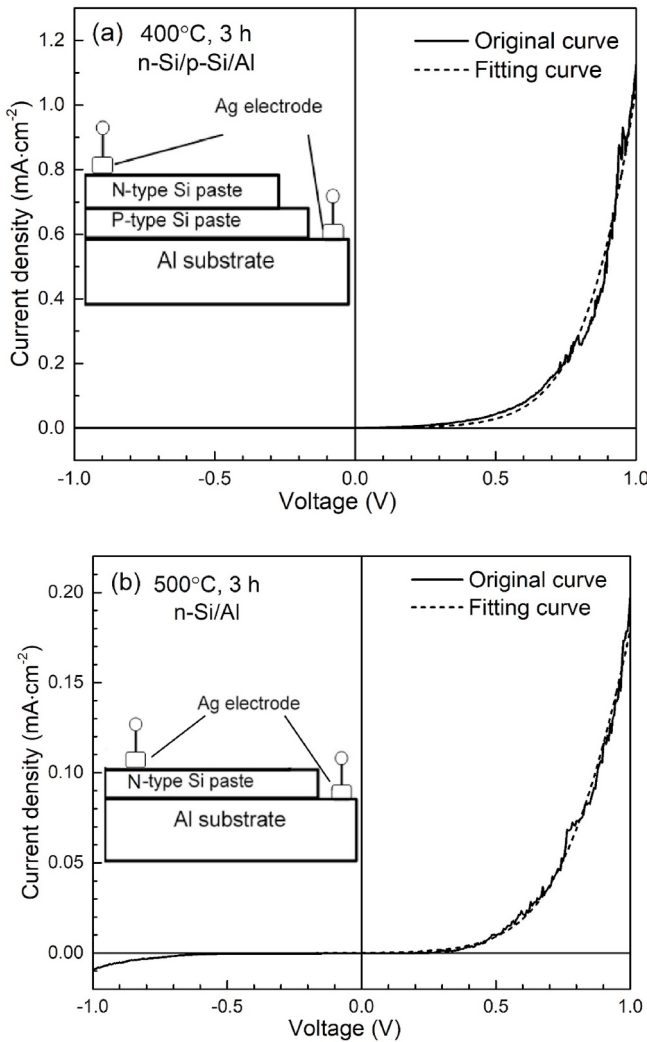


Fig. 5. I-V characteristics of the pn junction devices using the (a) p/n-type Si paste film annealed at 400 °C and the (b) n-type Si paste film annealed at 500 °C on Al substrates together with curve-fitting results (dash lines) using eq. (1).

using two Gaussian distribution functions is shown in Fig. 2 (c). The broad peak centered a lower wavenumber of 515 cm⁻¹ is attributed to small crystallites with diameters below 10 nm [27], rather than wurtzite phase [28], thus suggesting inclusion of a number of Si nanocrystals, as also shown later by SEM. The weak and broad feature centered at around 490 cm⁻¹ is referred to a-Si phase [29]. The a-Si phase could be formed in the instantaneous collision/friction among Si nanocrystals, miller wall, and milling beads. This a-Si phase surrounding Si nanocrystals like shells was so thin that the corresponding Raman peak was very weak [30]. After the annealing, this weak feature disappeared due to increasing crystallization of a-Si towards c-Si. Besides, there was another way of increasing crystallization. During the annealing, fine Si nanocrystals could be coalesced each other to grow and, eventually, form larger Si crystals.

The XRD patterns of the p-type Si paste films on Al substrates before and after annealing at 500 °C are shown in Fig. 3. The XRD patterns show some diffraction peaks of the underlying Al substrate. While weak diffraction peaks of Si are only observed before annealing, three distinct peaks assigned to Si (111), Si (220) and Si (311) appear after annealing. The increase in peak intensity of Si is due mainly to an increase in fraction of crystalline Si phase in the film after annealing via recrystallization. The FWHM of the Si (111) peak before and after annealing at

500 °C are measured to be 0.20° and 0.16°, respectively, thus confirming an increase in crystallinity by annealing. The diffraction patterns after annealing at other temperatures were almost similar.

Fig. 4 (a) shows the SEM image of the surface morphology of the p-type Si paste film on Al substrates annealed at 500 °C. Fig. 4 (b) and 4 (c) are the higher magnification image and the EDX spectrum of the square part of Fig. 4 (a), respectively. Fig. 4 (b) reveals that the film has porous structure and consists of grains with nominal sizes smaller than a few hundreds of nm. In particular, a large number of small grains with sizes below tens of nm exist. Fig. 4 (c) reveals that film surface consists dominantly of Si with small amounts of O, Fe, and C as impurities during the fabrication process. Hollow- or hole-like regions with sizes up to several micrometers are occasionally observed as shown typically in Fig. 4 (d). The EDX spectra for two positions marked with cross symbols 1 and 2 in Fig. 4 (d) are shown in Fig. 4 (e) and 4 (f), respectively. Fe and O peaks appear to come from ambient dusts because some particles containing only Fe and O were occasionally observed on the surface by SEM. As Fig. 4 (e) shows the presence of a considerable amount of Al, indicating that Al was driven to the surface by grain boundary diffusion. As the non-annealed Si film consists of nano-sized particle grains, the annealing process had a similar effect to sintering process of powder materials. There are two significant mass transport mechanisms during sintering, that is, grain boundary diffusion and lattice diffusion [23]. Al atoms are transported through grain boundaries into pores by the chemical potential gradient in the boundary plane, thus infilling the pores and densifying the film.

The I-V characteristic of a pn junction diode using a p/n-type double layer Si paste film on an Al substrate after annealing at 400 °C is shown in Fig. 5 (a), in which the device structure is depicted in the inset. The I-V characteristic shows rectification with an on/off current ratio corresponding to the rectification ratio of about 3200 @ ±1 V. The I-V characteristic is fitted using the standard equivalent circuit for the first-order diode modeling [31]. The total current at a given temperature (*T*) can be described by eq. (1) [32]:

$$I = I_s \left\{ \exp \left[\frac{q(V - IR_s)}{nkT} \right] - 1 \right\} \quad (1)$$

where *I*_s is the reverse saturation current, *q* is the elementary charge, *n* is the ideality factor, *k* is the Boltzmann constant, and *R*_s is the series resistance. Curve fitting results using eq. (1) are reasonably in agreement with the experimental data as shown in Fig. 5 (a). From the fitting result using eq. (1), the ideality factor is estimated to be about 4.3 with *R*_s = 1.8 kΩ. Such a high series resistance is attributed to a high defect density in Si paste films and an oxide layer surrounding each particle. The ideality factor is increased to about 4.8 at *R* = 4.0 kΩ when the annealing temperature is increased to 500 °C. This could be due to easier oxidation by higher temperature annealing, in agreement with the FT-IR results in Fig. 1 (a) and 1 (b). Besides, a preliminary test of the pn junction diode fabricated on an Al-sputtered Fe substrate by annealing at 500 °C showed a photo generated current density of 5.8×10^{-5} mA cm⁻² under AM1.5 illumination.

The I-V characteristic of a contact between an n-type single layer Si paste film and an Al substrate after annealing at 500 °C is shown in Fig. 5 (b). The I-V characteristic shows rectification with an on/off current ratio of about 23 @ ±1 V even without a p-type Si paste film. The result was similar when annealed at 400 °C. From the fitting result using eq. (1), the ideality factor is estimated to be 3.0 with *R*_s = 213 kΩ. This rectification characteristic is explained by Al impurity compensation near the interface of the n-type Si paste film and the Al substrate. Al serves as an acceptor and can form a p-type region in the n-type Si paste film when introduced at high concentrations through diffusion [33]. This indicates that a pn junction diode was formed in the n-type Si paste film by annealing. The series resistance of Eq. (1) using the n-type Si paste film is much higher than that using the p/n-type Si paste film. This is attributed to the much lower conductivity of the p-type region formed

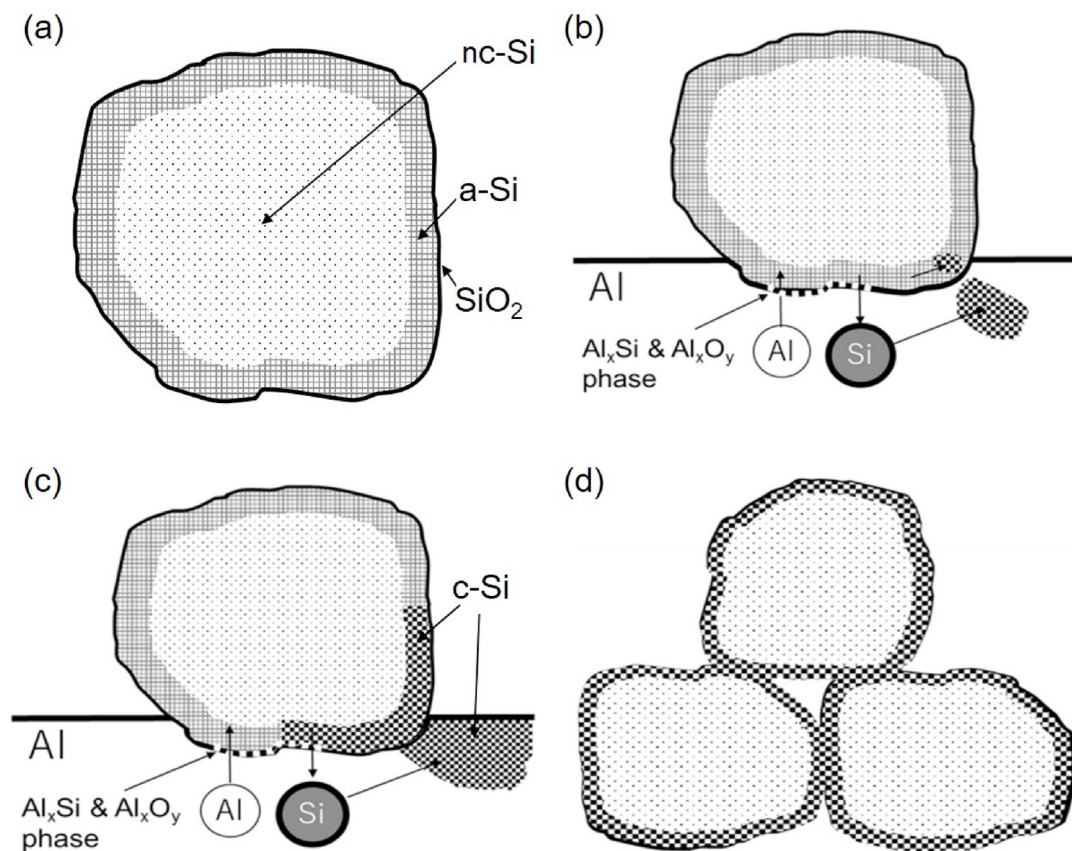


Fig. 6. Schematic diagrams of (a) a Si nano-crystallite structure in Si paste; (b) a first step of the AIC process: the reaction between Al and an oxide shell as well as the interdiffusion of Al and Si atoms; (c) a second step of the AIC process: nucleation and growth of Si; (d) Si particles contacting the neighboring particles without the oxide shell.

by Al compensation in the n-type paste film than that formed by B doping of the p-type wafer [34]. On the other hand, the I-V characteristics were found to exhibit almost linear relations typical of Ohm's law after annealing at 550 °C or above. This could be due to the loss of pn junction structure by excess Al diffusion into the n-type paste film from the Al substrate as shown by the EDX results.

As shown in the FTIR, XRD and SEM results, the Si paste films still showed some voids and slight oxidation, which may degrade performance of the resulting devices. Further work should be focused on reduction of voids, defects, and oxidation, in particular, at grain boundaries to improve performance of pn junctions using our method. One of the possible approaches of improvement is reduction of oxidation by introducing Ti [35]. Moreover, such inert substrates as quartz or even glass typically used in AIC process should be tested for pn junction formation. For manufacturing Si paste directly by Si chunk instead of fragments of doped Si wafers, doping during ball milling of the Si chunks should also be studied.

Models are introduced in the following to explain the possible mechanism of improving crystallinity of Si paste films by the AIC process. During the ball milling process, crushed nano-crystalline Si (nc-Si) particles are surrounded by a very thin a-Si shell and also oxidized to some degree, forming the so-called core-shell structure [36], as illustrated in Fig. 6 (a). In the meantime, as the size of the nc-Si decreases, the specific surface area will increase drastically. Therefore, the nc-Si can readily react with oxygen, making the particles vulnerable for oxidation. The oxide SiO_x is not favorable because it is an insulator and strongly impairs the conductivity of the Si paste film.

Inspired by the AIC process for nucleation and diffusion-controlled crystal growth at the Al/a-Si interface [14], schematic diagrams of the possible mechanism in our Si paste films are depicted in Fig. 6 (b)-6 (d).

Since the Si paste film is coated and pressed on an Al substrate, the Si particle in the film has a core shell structure in the order of Al/SiO₂/a-Si/nc-Si from the outer to the inner of the particle as shown in Fig. 6 (b). When the Si paste film is annealed at a low temperature of around 400–500 °C, a part of the Si oxide shell reacts with Al. The products of this reaction should be Al_xSi and Al_xO_y [37], and Al_xSi plays a role of a channel through which Al and Si atoms could diffuse each other. The Si atoms in a-Si phase diffuse outward into the Al layer and further form Al_xSi. Concurrently, Si clusters start growing inside and outside of the oxide shell during the annealing. The Al atoms also diffuse inwards into the a-Si/nc-Si shell at the same time as shown in Fig. 6 (b). Since Al is known as a p-type dopant rather than a deep-level impurity in Si, a p⁺ type Al layer is expected to be formed in the p-type Si layer. The Si atoms diffused from a-Si phase are gradually transformed into crystalline phase as shown in the thick hatched c-Si region in Fig. 6 (c). Then, the oxide shell gets thinner in this step. It should be noted that the reaction between the oxide shell and Al does not happen only at the bottom side of the particle that touches the Al layer because the Al diffuses closer to the surface region as indicated by EDX in Fig. 4 (e). The whole oxide shell tends to react with Al. In the last step of AIC as shown in Fig. 6 (d), most of the a-Si transforms into c-Si and the oxide shell disappears. As the c-Si region continues to grow, the Si particle starts contacting the neighboring particles directly owing to the absence of the oxide shell. The contacting areas between Si particles could become conductive routes for the carriers.

4. Conclusion

A metal-induced crystallization technique using Al as the metal species was utilized for enhancing recrystallization of nanocrystalline Si

paste films on Al substrates by annealing at low temperatures (400–550 °C). This low-temperature annealing process reduced the residual tensile stress and the oxidation of the Si paste films greatly as confirmed by FTIR, Raman spectroscopy, and XRD, contrastive to the conventional high-temperature annealing process above 1000 °C. A pn junction diode using a p/n-type double layer Si paste film on an Al substrate after annealing at 400 °C showed the rectifying I-V characteristic with the on/off current ratio of about 3200 @ ±1 V, and the reverse current density was low enough at $1.8 \times 10^{-9} \text{ A/cm}^2$ @ -1 V. The rectifying I-V characteristic typical of a pn junction diode was also observed using an n-type single layer Si paste film on an Al substrate after annealing at 400–500 °C, indicating the formation of a p-type region in the Si paste film by Al compensation.

CRediT authorship contribution statement

Yusuke Kuboki: Methodology, Validation, Investigation, Writing – original draft. **Huan Zhu:** Investigation, Writing – review & editing. **Morihiro Sakamoto:** Investigation, Methodology. **Hiroshige Matsumoto:** Resources, Methodology. **Kungen Teii:** Writing – review & editing. **Yoshimine Kato:** Conceptualization, Supervision, Writing – review & editing.

Declaration of competing interest

The authors declare that they have no known competing financial interests or personal relationships that could have appeared to influence the work reported in this paper.

Acknowledgement

This work was supported in part by JSPS KAKENHI Grant Number JP16K13720. The authors would like to thank Prof. Satoru Tanaka, Mr. Hagiwara, Prof. Hiroaki Nakano, and Mr. Satoshi Ooue for lending us their experimental facilities.

References

- [1] H. Chang, S.Q. Sun, Si nanoparticles: preparation, properties, and applications, *Chin. Physica B* 23 (8) (2014), 088102.
- [2] S.S. Rink, D.A.B. Miller, D.S. Chemla, Theory of the linear and nonlinear optical properties of semiconductor microcrystallites, *Phys. Rev. B* 35 (15) (1987) 8113–8125.
- [3] A.C. Arias, J.D. MacKenzie, I. McCulloch, J. Rivnay, A. Salleo, Materials and applications for larger area electronics: solution-based approaches, *Chem. Rev.* 110 (2010) 3–24.
- [4] M.G. Panthani, B.A. Korgel, Nanocrystals for electronics, *Annu. Rev. Chem. Biomol. Eng.* 3 (2012) 287–311.
- [5] R.A. Street, Technology and Applications of Amorphous Silicon, Springer, New York, 2000.
- [6] S. Nishizaki, K. Ohdaira, H. Matsumura, Comparison of a-Si TFTs fabricated by Cat-CVD and PECVD methods, *Thin Solid Films* 517 (2009) 3581–3583.
- [7] Y. Gao, S. Zhou, Y.F. Zhang, C. Dong, X.D. Pi, D.R. Yang, Doping silicon wafers with boron by use of silicon paste, *J. Mater. Sci. Technol.* 29 (2013) 652–654.
- [8] Y. Tomizawa, T. Immamura, M. Soeda, Y. Ikeda, T. Shiro, Laser doping of boron-doped Si paste for high-efficiency silicon solar cell, *Jpn. J. Appl. Phys.* 54 (2015), 08KD06.
- [9] O.V. Roos, A simple theory of back surface field (BSF) solar cells, *J. Appl. Phys.* 49 (1978) 3503–3511.
- [10] Y. Li, H. Inokuchi, T. Orita, K. Maejima, K. Nakashima, S. Ooue, H. Matsumoto, Y. Kato, PN junction formation by Si paste coated on metal substrates, *J. Mater. Sci. Mater. Electron.* 30 (2019) 6693–6700.
- [11] H. Zhu, M. Sakamoto, T. Pan, T. Fujisaki, H. Matsumoto, K. Teii, Y. Kato, Rapid thermal annealing of Si paste film and pn-junction formation, *Nanotechnology* 31 (2020) 385202.
- [12] W. Knaepen, C. Detavernier, R.L. Van Meirhaeghe, J. Jordan Sweet, C. Lavoie, In-situ X-ray diffraction study of metal induced crystallization of amorphous silicon, *Thin Solid Films* 516 (2008), 4946–952.
- [13] A.K. Volk, N. Tucher, J. Seiffe, H. Hauser, Ma Zimmer, B. Bläsi, M. Hofmann, J. Rentsch, Honeycomb structure on multi-crystalline silicon Al-BSF solar cell with 17.8% efficiency, *IEEE J. Photovolt.* 5 (2015) 1027–1033.
- [14] O. Nast, S.R. Wenham, Elucidation of the layer exchange mechanism in the formation of polycrystalline silicon by aluminum-induced-crystallization, *J. Appl. Phys.* 88 (2000) 124–132.
- [15] D.A. Porter, K.E. Easterling, Phase Transformations in Metals and Alloys, Chapman and Hall, New York, 1992.
- [16] P.G. Pai, S.S. Chao, Y. Takagi, G. Lucovsky, Infrared spectroscopic study of SiO_x films produced by plasma enhanced chemical vapor deposition, *J. Vac. Sci. Technol. A* 4 (1986) 689–694.
- [17] G. Lucovsky, J. Yang, S.S. Chao, J.E. Tyler, W. Czubatyj, Oxygen-bonding environments in glow-discharge-deposited amorphous silicon-hydrogen alloy films, *Phys. Rev. B* 28 (1983) 3225–3233.
- [18] X.D. Pi, L. Mangolini, S.A. Campbell, U. Kortshagen, Room-temperature atmospheric oxidation of Si nanocrystals after HF etching, *Phys. Rev. B* 75 (2007), 085423.
- [19] G. Lucovsky, C.K. Wong, W.B. Pollard, Vibrational properties of glasses: intermediate range order, *J. Non-Cryst. Solids* 59–60 (1983) 839–846.
- [20] E.A. Irene, D.W. Dong, Silicon oxidation studies: the oxidation of heavily B- and P-doped single crystal silicon, *J. Electrochem. Soc.* 125 (1978) 1146–1151.
- [21] Y. Ishikawa, Thermal oxidation of antimony-doped silicon, *Jpn. J. Appl. Phys.* 41 (2002) 1986–1987.
- [22] D.L. Johnson, T.M. Glarke, Grain boundary and volume diffusion in the sintering of silver, *Acta Metall.* 12 (1964) 1173–1179.
- [23] F.B. Swinkels, M.F. Ashby, Role of surface redistribution in sintering by grain boundary transport, *Powder Metall.* 23 (1980) 1–6.
- [24] R.E. Mistler, R.L. Coble, Grain-boundary diffusion and boundary widths in metals and ceramics, *J. Appl. Phys.* 45 (1974) 1507–1509.
- [25] H.J.T. Ellingham, Reducibility of oxides and sulphides in metallurgical processes, *J. Soc. Chem. Ind.* 63 (1944) 125–160.
- [26] Q. Li, W. Qiu, H. Tan, J. Guo, Y. Kang, Micro-Raman spectroscopy stress measurement method for porous silicon film, *Opt. Laser. Eng.* 48 (2010) 1119–1125.
- [27] M.N. Islam, S. Kumar, Influence of crystallite size distribution on the micro-Raman analysis of porous Si, *Appl. Phys. Lett.* 78 (2001) 715–717.
- [28] R.J. Kobliska, S.A. Solin, Raman spectrum of wurtzite silicon, *Phys. Rev. B* 8 (1973) 3799–3802.
- [29] R.L.C. Vink, G.T. Barkema, W.F. van der Weg, Raman spectra and structure of amorphous Si, *Phys. Rev. B* 63 (2001) 115210.
- [30] Y.C. Wang, W. Zhang, L.Y. Wang, Z. Zhuang, E. Ma, J. Li, Z.W. Shan, In situ TEM study of deformation-induced crystalline-to-amorphous transition in silicon, *NPG Asia Mater.* 8 (2016) e291.
- [31] M. Meseth, P. Ziolkowski, G. Schierning, R. Theissmann, N. Petermann, H. Wiggers, N. Benson, R. Schmeichel, The realization of a pn-diode using only silicon nanoparticles, *Scripta Mater.* 67 (2012) 265–268.
- [32] S.M. Sze, K.K. Ng, Physics of Semiconductors Devices, Wiley-Interscience, New Jersey, 2007.
- [33] C.S. Fuller, J.A. Ditzingerberger, Diffusion of donor and acceptor elements in silicon, *J. Appl. Phys.* 27 (1956) 544–553.
- [34] L.E. Ramos, E. Degoli, G. Cantele, S. Ossicini, D. Ninno, J. Furthmüller, F. Bechstedt, Structural features and electronic properties of group-III-, group-IV-, and group-V-doped Si nanocrystallites, *J. Phys. Condens. Matter* 19 (2007) 466211.
- [35] H. Zhu, T. Pan, L. Majula, H. Matsumoto, and Y. Kato, $\text{TiO}_2/\text{p-Si}$ paste heterojunction fabricated by rapid thermal annealing, *Appl. Surf. Sci.*, to be published.
- [36] G. Schierning, R. Theissmann, N. Stein, N. Petermann, A. Becker, M. Engenhorst, V. Kessler, M. Geller, A. Beckel, H. Wiggers, R. Schmeichel, Role of oxygen on microstructure and thermoelectric properties of silicon nanocomposites, *J. Appl. Phys.* 110 (2011) 113515.
- [37] J.H. Kim, J.Y. Lee, Al-induced crystallization of an amorphous Si thin film in a polycrystalline Al/native SiO_2 /amorphous Si structure, *Jpn. J. Appl. Phys.* 35 (1996) 2052–2056.